A Low-Energy Emulsification Batch Mixer for Concentrated Oil-in-Water Emulsions

Sylvain Caubet
Institut Pluridisciplinaire de Recherche Environnement et Matériaux (IPREM UMR 5244), Equipe de Physique et Chimie des Polymères (EPCP), Université de Pau et des Pays de l'Adour (UPPA), Hélioparc, Avenue P. Angot, 64000 Pau, France

Laboratoire de Thermique Energétique et Procédés (LaTEP), Université de Pau et des Pays de l'Adour (UPPA), IFR, BP 7511, 64075 Pau cedex, France

Yves Le Guer
Laboratoire de Thermique Energétique et Procédés (LaTEP), Université de Pau et des Pays de l'Adour (UPPA), IFR, BP 7511, 64075 Pau cedex, France

Bruno Grassl
Institut Pluridisciplinaire de Recherche Environnement et Matériaux (IPREM UMR 5244), Equipe de Physique et Chimie des Polymères (EPCP), Université de Pau et des Pays de l'Adour (UPPA), Hélioparc, Avenue P. Angot, 64000 Pau, France

Kamal El Omari
Laboratoire de Thermique Energétique et Procédés (LaTEP), Université de Pau et des Pays de l'Adour (UPPA), IFR, BP 7511, 64075 Pau cedex, France

Eric Normandin
Plateau Innov'Adour (UPPA), Université de Pau et des Pays de l'Adour (UPPA), Hélioparc, Avenue P. Angot, 64000 Pau, France

DOI 10.1002/aic.12253
Published online April 20, 2010 in Wiley Online Library (wileyonlinelibrary.com).

This work shows the formation of a high internal phase ratio oil-in-water (O/W) emulsion using a new type of a two-rod batch mixer. The mixture components have sharply different viscosities [1/3400 for water-in-oil (W/O)], similar densities (1/0.974 for W/O), and an O/W ratio of 91% (wt/wt). The simple design of this mixer leads to a low-energy process (10^6 < energy density [J m^{-3}] < 10^7), characterized by low rotational speed and laminar flow. The droplet size distribution during the emulsification was investigated according to different physical and formulation parameters such as stirring time (few minutes < t < 1 h), rotational speed (60 < Ω < 120 rpm), surfactant type (Triton X-405 and X-100), concentration (from 1 to 15.9 wt % in water), and salt addition (30 g/L). We show that all studied parameters allow a precise control of the droplet size distribution and the rheology. The resulting emulsions are unimodal and the mean droplet diameter is between 30 μm and 8 μm. © 2010 American Institute of Chemical Engineers *AIChE J,* 57: 27–39, 2011
Keywords: batch mixer, laminar flow emulsification, concentrated emulsions, droplet size distribution control, rheokinetics

Correspondence concerning this article should be addressed to Y. Le Guer at yves.leguer@univ-pau.fr.

Introduction

To disperse a fluid into another immiscible fluid, some mechanical energy, for example, shear, is applied, together with a surfactant, to produce a dispersion with stable properties, including final droplet size, polydispersity, and rheology. The nature of the two fluids, the surfactant, and the process conditions (design of the mixer, mixing rate, and time) all have a critical effect on the properties of the final emulsion. During the process of emulsification, external shear energy is used to break large drops into smaller ones. For an internal volume ratio above 0.74, emulsions are called high internal phase ratio (HIPR) emulsions, biliquid foam systems, or gel emulsions.[1] HIPR emulsions are encountered in a wide variety of industrial applications: petrochemical for bitumen or heavy crude oils,[2] agrochemicals, pharmaceuticals, cosmetics, etc. The main works of Princen[3,4] have described the rheological and structural properties of gel emulsions. Most of the proprieties of gel emulsions, particularly their rheological behaviors, are affected by the droplet size distribution, the volume fraction, and the interfacial tension between oil and water.[5,6] Thus, during the emulsification process, the droplet size distribution is an important parameter to control to obtain a HIPR emulsion with the desired properties. This depends on several parameters, such as the process, the surfactant, the water/oil ratio, the type of oil (vegetable, synthetic, bitumen, etc.), and other formulation and physical parameters used for the mixing. Typically, the droplet diameter can vary from one to hundreds of micrometers. Rheological studies concerning emulsions have only begun recently and are mostly concerned with ''dispersed'' emulsions (with an internal volume ratio lower than 0.74), whereas most of HIPR emulsion studies are made on water-in-oil (W/O) emulsions.[7,8] HIPR inverse emulsions (O/W), which are considered in this work, generally have a shear thinning behavior with viscosity ranging from a few to several thousand Pa s as a function of the shear rate, the droplet size distribution, and the internal volume ratio.[9–11]

There is a range of commercially available equipment that can be used to produce HIPR oil-in-water (O/W) emulsions, for example, coaxial mixers[12]; colloid mills[13]; high-pressure homogenizers[14]; and static mixers.[15] The production of such emulsions is also possible by the use of a complex thermodynamic mechanism, which uses the inversion phenomenon as detailed elsewhere.[16] Of course, this list is not exhaustive; other methods and apparatus exist for preparing HIPR O/W emulsions.

In this work, we present a new type of batch mixer that, contrary to the aforementioned equipment, uses a very simple geometry (with circular rods and a tank) and which can be easily extended to a continuous process. This mixer uses a laminar flow with rather moderate rotational speeds that makes it suitable for emulsification of highly viscous fluids (such as heavy oils in petroleum industries). Another novel attribution to this mixer is its one-step operating mode and the resulting emulsification procedure that starts with the tank filled with a high ratio phase (oil) that disperses into the low ratio phase (water and surfactant). Here, the issue of mixing effects on the size, distribution, and stability of concentrated O/W emulsions with contrasting viscosities (1/3400 for W/O) and similar densities (1/0.974 for W/O) is addressed for a new type of laminar batch mixer. The HIPR emulsions are made in a batch two-rod mixer (TRM) at a high volume ratio (0.91) of castor O/W. We investigate how the droplet size distribution is affected by the variation of physical and formulation parameters such as stirring time, rotational speed, surfactant type, and its concentration, and addition of salt. Rheological behaviors are also presented.

Materials and Methods

Materials

The oil used is blown castor oil from Seatons (Ricin oil). It was chosen mainly for its high density (974 kg m^{-3}) and high viscosity (3.4 Pa s at 20°C). Two well-known nonionic surfactants were used and compared as follows: Triton X-405 (HLB = 17.9, CMC in water of 0.159 [wt/wt], product of Sigma-Adrich) and Triton X-100 (HLB = 13.5, CMC in water of 0.018 [wt/wt], product of Sigma-Aldrich).[17,18] Deionized water, with an electrical conductivity of 18.3 MΩ cm, was filtered through a 0.22-μm Millipore filter. Sodium chloride (NaCl) was obtained from Sigma-Aldrich.

Emulsion preparation

The experimental setup used to produce the HIPR emulsion was a batch TRM (Figures 1a,b). The larger rod was not coaxial with the tank and its rotational speed was controlled by a computer. A second, smaller, rod, not rotating, was located next to the first one. The geometrical parameters were as follows: tank diameter (d') = 150 mm, larger rod radius (r) = 50 mm, smaller rod diameter (d'') = 15 mm, rod–tank gap (ε) = 3 mm, rod–rod gap (ε') = 2 mm, and the angular position of the smaller rod (θ) = 30° (Figure 1b). These geometrical parameters remained the same for all of the experiments considered in this study. A system with a strength sensor was adapted to the motor of the larger rod to follow the evolution of the resistive torque during the emulsification process. The calculation of the torque and, thus, of the power input to keep the rotational speed constant can be calculated using the following relations:

$$C = F \cdot a \tag{1}$$

$$P = C \cdot \omega \tag{2}$$

where F is the measured strength in Newton; a, the distance between the sensor and the axis of the motor ($a = 0.185$ m); C, the torque (N m); ω, the angular velocity of the larger rod (rad s^{-1}); and P, the power (W).

The protocol used to produce the HIPR O/W emulsion is as follows. First, 400 mL of castor oil was added to the tank. Then, the larger rod was rotated at the selected rotational speed (Ω = 60, 90, or 120 rpm). Finally, after 1 min, 38.6 mL of a mixture of distilled water and surfactant was rapidly added into the TRM batch process. The emulsification began at time $t = 0$ s when the water–surfactant mixture is added in the tank. The emulsification can then be divided into three steps. First, the water–surfactant mixture is introduced into the tank. Rapidly thereafter (after a few seconds), the emulsification begins, droplets of oil are formed in the water phase, and all of the castor oil is gradually dispersed in the water. A crude emulsion is then created, which leads to

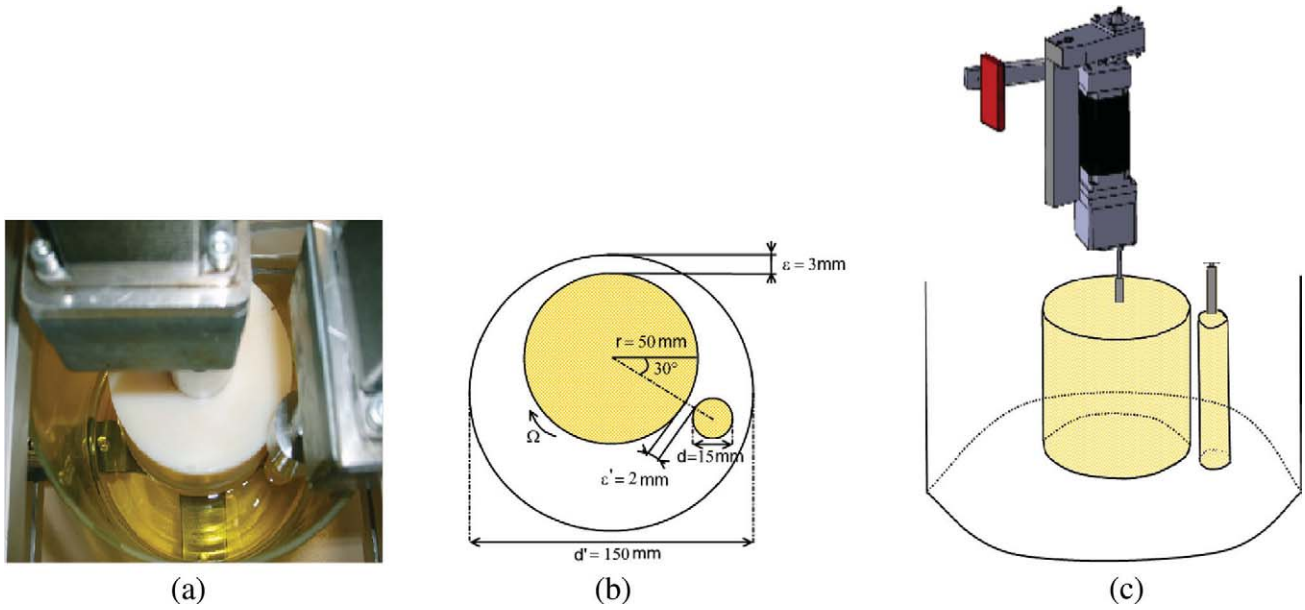

Figure 1. (a) Photo of the two-rod mixer (TRM) batch device; (b) Schematic of the TRM batch with the dimensions of the elements; and (c) 3D view of the TRM equipped with a strength sensor.

[Color figure can be viewed in the online issue, which is available at wileyonlinelibrary.com.]

the formation of the first monodisperse emulsion. The duration (t_0) that corresponds to the creation of this primary monodisperse emulsion ranges between 1 and several minutes and depends, in particular, on the rotational speed of the larger TRM rod (see section "Effect of rotational speed on the final diameter"). This initial time t_0 is an important characteristic time because it represents the limit between two regimes in the evolution of the mean droplet diameter as a function of the mixing time.[19] In the last step, the droplets of the initial monodisperse emulsion are gradually broken into smaller ones. This mechanism induces a reduction of the mean diameter until a limit value is reached (see section "Effect of the mixing time on the mean diameter").

During the process, the temperature was measured in situ and its variation (in °C) did not exceed 10% of its initial value for all studied rotational speeds. Emulsions were prepared at room temperature (20°C ± 1°C) at various rotational speeds (60, 90, and 120 rpm) for total mixing times of 1 h. At no point during the experiments did the temperature exceed 22°C.

Determination of droplet size distribution

The droplet size distribution was determined via optical microscopy according to the method described by Tcholakova et al.[20] The samples, carefully taken from the TRM with a syringe not to disturb the mixing, were immediately transferred to 4 wt % Triton (X-405 or X-100) solutions to prevent further drop coalescence and to reduce the droplet concentration to about 3 vol % because the original emulsion was too concentrated for droplet size analysis (cf. Figure 2). This dilution was transferred for optical examination into microcapillaries with rectangular cross sections (depth 0.2 mm, width 0.7 mm, and length 1 mm) not more than 1 h after their preparation. Before loading the sample into the microcapillary, the vial containing the Triton-stabilized emulsion was gently rotated to homogenize the emulsion. The oil droplets were observed via transmitted light microscopy with a Leica DMLM microscope (magnification ×20) connected to a charge-coupled device camera (Leica DFC280) and video recorder software (Leica IM4.0).

The diameters of individual recorded oil droplets were measured using the publicly available software ImageJ 1.40, released by the National Institute of Health (http://rsb.info.nih.gov/ij/index.html). These data were numerically processed to obtain droplet size histograms. The diameters of at least 800 droplets were measured for each system. Illustrative droplet size histograms are shown in Figure 3.

The mean diameter (d_m), the mean volume–surface diameter (the Sauter diameter, d_{32}), and the uniformity factor (U) were calculated from the following relations:

$$d_m = \frac{\sum n_i d_i}{\sum n_i} \tag{3}$$

$$d_{32} = \frac{\sum n_i d_i^3}{\sum n_i d_i^2} \tag{4}$$

$$U = \frac{1}{d^*} \frac{\sum n_i d_i^3 |d^* - d_i|}{\sum n_i d_i^3} \tag{5}$$

where n_i is the number of droplets of diameter d_i and d^* is the median diameter (the diameter for which the cumulative undersize volume fraction is equal to 0.5). Emulsions are considered to be monodisperse if U is smaller than 0.25.[19]

Rheological measurements

The steady shear rheological properties of the HIPR emulsion were measured using a Malvern Bohlin C-VOR 150 rheometer

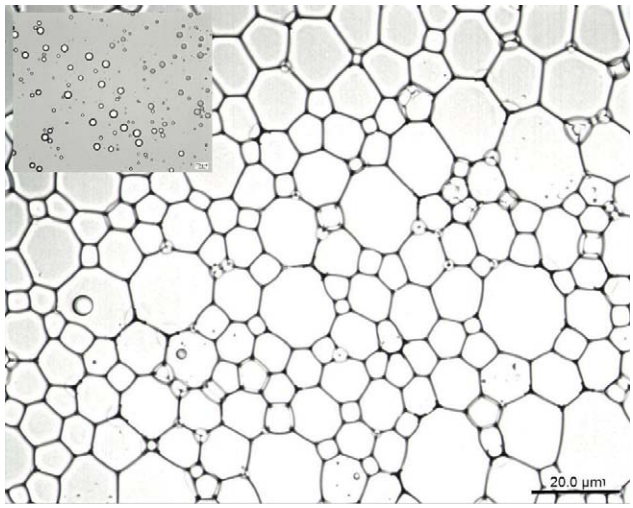

Figure 2. Optical photomicrograph of concentrated emulsion obtained using the batch two-rod mixer process after 780 s of mixing with a rotational speed of the rod equal to 90 rpm.

The surfactant used was 15.9 wt % Triton X-405 in water. Inset: optical photomicrograph after dilution. In both cases, the scale bar is 20 μm. [Color figure can be viewed in the online issue, which is available at wileyonlinelibrary.com.]

in controlled stress mode with a cone plate geometry (diameter of 60 mm and cone angle of 2°). Stepped shear stress values were selected to study shear rates ranging from 0.1 to 100 s^{-1}. The system was allowed to reach steady state at each shear stress before registering the measured values. The measurements were performed by increasing and decreasing the shear stress. Temperature was controlled with a Peltier plate system and was set at 20.0°C ± 0.1°C. Dynamic frequency sweep tests were recorded in stress mode at 5 Pa, which was kept constant over the frequency range of 0.1–30 Hz at 20°C. For all experiments, a linear regime was used.

Interfacial tension measurements

A drop tensiometer (Tracker, IT Concept) was used to measure the interfacial tension by analyzing the axisymmetric shape (Laplacian profile) of a rising castor oil drop in aqueous surfactant solution at 20°C ± 0.5°C.

Results and Discussion

Effect of the mixing time on the mean diameter

In this study, the emulsion was made using a 15.9 wt % solution of Triton X-405 in distilled water as described in section "Emulsion preparation." For this experiment, the rotational speed of the rod remained constant and equal to 90 rpm throughout the process. During the emulsification, samples were taken at times t = 300, 420, 780, 1140, 2400, and 3600 s. The droplet size distribution was then determined and its probability distribution was plotted for each sampling time. All size distributions of the HIPR emulsions were unimodal and could be considered as being monodisperse on the basis of the definition of monodispersity, that is, a uniformity factor U is smaller than 0.25 (according to Eq. 5).

The evolution of the mean diameter during the mixing over one experiment is shown in Figure 4. Two particular points can be distinguished in the evolution of the curve. First, the mean diameter decreases rapidly from 23 μm (t = 180 s) to 15 μm (t = 780 s); that is, in 600 s, d_m has been diminished by 8 μm. Then, at the second point in time, the mean diameter decreases slowly from 15 μm (t = 780 s) to a limiting value of 11 μm (t = 2400 s); that is, in 1620 s, the mean diameter has only been diminished by 4 μm.

To obtain more details concerning the flow patterns in the TRM, we performed a numerical simulation in a horizontal section of the mixer. We resolved the equations governing the flow, that is, equations of conservation of mass and momentum. We chose to focus on the flow of a concentrated emulsion for a given droplet distribution exhibiting a non-Newtonian behavior and approached the problem by using a shear-thinning power-law model, wherein the viscosity is a function of shear rate as follows:

$$\eta(\dot{\gamma}) = k\dot{\gamma}^{n-1} \tag{6}$$

Here, the values of n and k are obtained from the experimental rheological characterization of the emulsion obtained for a mixer rotating at Ω = 90 rpm after a mixing time of 2400 s (see Figure 10 for $\dot{\gamma} > 10\ s^{-1}$). The rheological characterization of the emulsion is presented below in the experimental section entitled "Effect of the mean droplet diameter on the rheological behavior."

The resolution of this problem involves the use of an unstructured Finite Volume method with second order accurate spatial schemes. The pressure–velocity coupling is ensured by SIMPLE algorithm. Complete details on the code and numerical procedures can be found in El Omari and Le Guer.[21,22] The two-dimensional computational mesh contains 33,000 cells.

We present in Figure 5a the obtained streamlines of the flow for the aforementioned parameters. We can observe a large and a small recirculations located at each side of the nonrotating smaller rod. The fluid velocities (not shown here) are important only in a limited region around the rotating rod and outside this zone, the fluid flows at lower velocities. This is due to shear-thinning behavior of the fluid: its viscosity is reduced near the large rod and the emulsion is well driven by the flow only there. As a consequence, the center of the large recirculation is located near the rotating rod.

The Figure 5b shows the distribution of the shear rate $\dot{\gamma}$ in the mixer. The shear rate is expressed as follows:

$$\dot{\gamma} = \sqrt{2\,tr(\overline{\overline{D}}^2)} \text{ with } \overline{\overline{D}} = \frac{1}{2}\left(\overline{\overline{\nabla}}\,V + \left(\overline{\overline{\nabla}}\,V\right)^T\right)$$

the rate of deformation tensor.

High shear rate values are found around the rotating rod with maximum values located in the two gaps. To characterize the non-Newtonian flow, a generalized Reynolds number is defined for the power-law model:

$$Re_{PL} = \frac{\rho(d' - 2r)^n}{k\,V_f^{n-2}} \tag{7}$$

with n = 0.355 and k = 51.662 (for 2400 s mixing time) Re_{PL} is equal to 1.88. This value of the generalized power-law

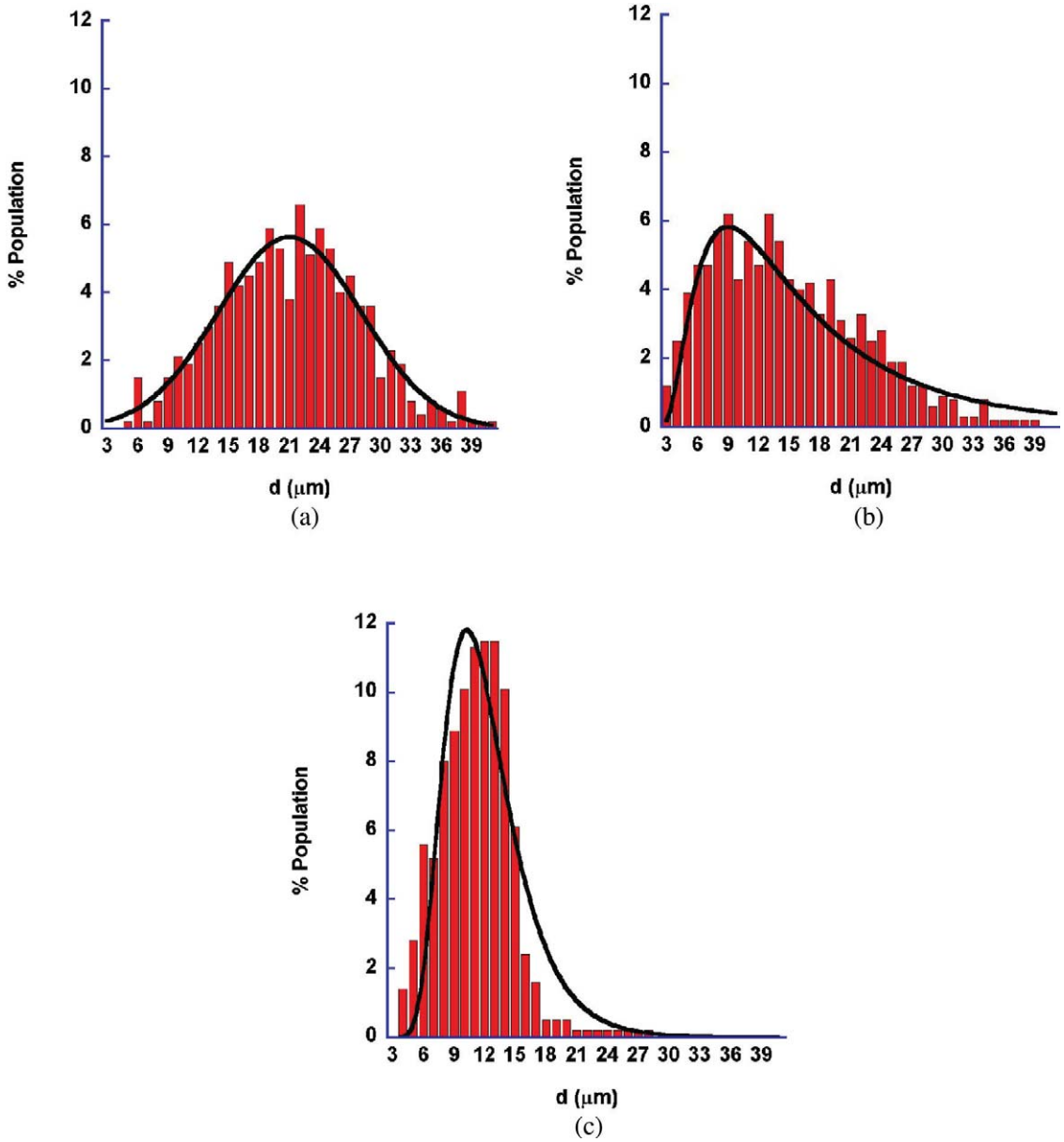

Figure 3. Evolution of the droplet size distribution during the emulsification in the TRM batch process at a rotational speed of the rod equal to 90 rpm.

After (a) 300, (b) 780, and (c) 2400 s of mixing. The surfactant used was 15.9 wt % Triton X-405 in water. Fit (black curves) was made using (a) Gaussian (normal) distribution; (b) and (c) log normal distribution. [Color figure can be viewed in the online issue, which is available at wileyonlinelibrary.com.]

Reynolds number demonstrates the highly viscous laminar flow conditions.

It is in the two intervening regions between the cylinders that the elongation and shear of the oil operates to produce the break-up mechanism, which results in the formation of droplets. As it is shown from the shear rate distribution of Figure 5b, the two zones that are the most favorable for the break-up mechanism are extremely localized (rod–rod and rod–tank gaps). This implies that the fluid can spend a relatively long time in the mixer before being able to pass in these two zones; thus, the kinetics of emulsification is difficult to predict.

A crude emulsion can be transformed into a monodisperse one, as shown by Mason and Bibette[23] who have experimentally discovered this phenomenon by applying a shear step to a crude emulsion. Moreover, Mabille et al.[19] have shown that the fragmentation kinetics of a calibrated emulsion as a function of the initial droplet size involves two distinct regimes. Over short times, the droplet diameter decreases abruptly. The droplets deform into long threads that undergo Rayleigh instability. During this regime, the obtained diameter is mainly determined by the applied stress and weakly depends on the viscosity ratio between the dispersed and continuous phases. After this first step, the resulting droplets

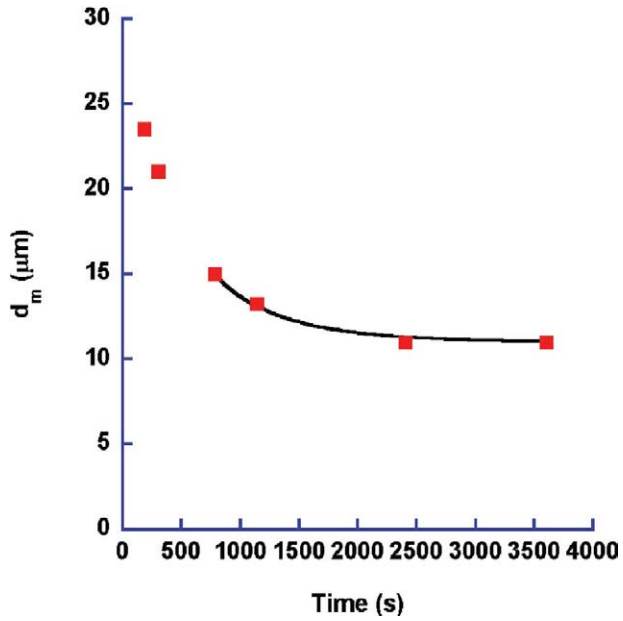

Figure 4. Evolution of the mean droplet diameter during mixing.

Points are experimental data, and the line is fitted to experimental data by the use of Eq. 9. [Color figure can be viewed in the online issue, which is available at wileyonlinelibrary.com.]

can, once again, break up into daughter droplets. This second mechanism is much slower with a characteristic duration of several hundred seconds. Depending on the initial size, the first step can vanish and only the second slow step persists. In addition to the influence of the fluid properties and the type of the flow, this phenomenon is also influenced by the degree of flow confinement,[24,25] which is not uniform in our mixer due to eccentricity.

In our process, if the crude emulsion was mainly composed of large drops, even after a few seconds of shear, we obtained a well-calibrated emulsion (with a mean diameter close to 24 μm); all the drops deformed into threads of different lengths, and the Rayleigh instability occurs when the critical radius is reached by each thread. Subsequently, when the first monodisperse emulsion was obtained, the second slow mechanism took place and as the smaller droplets (between d_0 and d_s defined below) also broke up, the size distribution became even narrower in the second regime. However, it is clear that the most efficient process to obtain narrow size distributions is the initial Rayleigh instability.

To model the second slow regime, Mabille et al.[19] considered that one droplet breaks into $r + 1$ daughter droplet per unit time until the final (saturating) diameter is reached. Then, the variation of the number of droplets is expressed using $dn = r\ n(t)\ dt$. Considering that this parameter r is a function of the mother droplet diameter, they adopted an empirical relation to express r as a function of the mother droplet diameter (d) as in: $r = r_0 \frac{d-d_s}{d_s}$. Writing the volume conservation during break up, they obtained Eq. 8 that models the evolution of the diameter during the slow regime.

$$d_m(t) = \frac{d_s}{1 - \frac{d_0 - d_s}{d_0} \exp\left(-\frac{r_0 t}{3}\right)} \tag{8}$$

In this equation, d_0 is the diameter of the initial monodisperse emulsion in the slow regime, d_s is the saturating diameter, and r_0 is the rupture rate whose significance is discussed below.

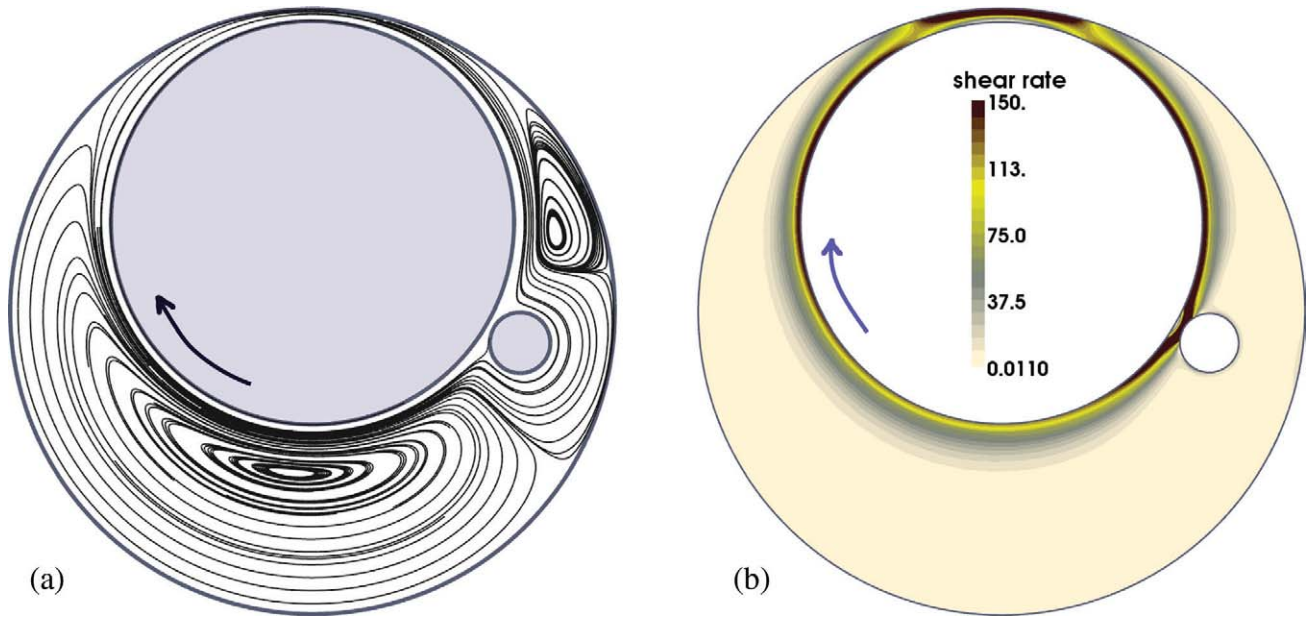

Figure 5. Flow simulation results for an angular rotating velocity Ω = 90 rpm.

(a) Flow streamlines; (b) distribution of the shear rate $\dot{\gamma}$ in the mixer section (a maximum localized value of 844 s^{-1} obtained for the smaller gap (ε'). The maximum value of the color scale was fixed to 150 for clarity. [Color figure can be viewed in the online issue, which is available at wileyonlinelibrary.com.]

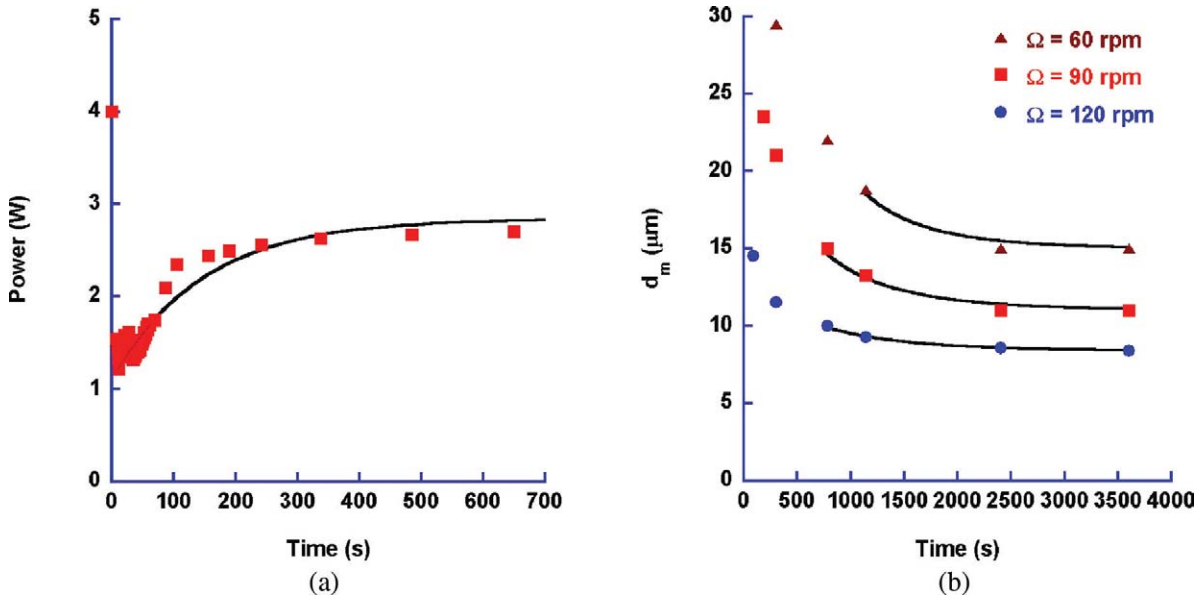

Figure 6. (a) Evolution of power during the emulsification for different rotational speeds of the rod (circles: Ω = 120 rpm, squares: Ω = 90 rpm, and triangles: Ω = 60 rpm). Curve fits were obtained using Eq. 11. At time 2400 s, the generalized power-law Reynolds number Re_{PL} associated to each rotational speed are 1.38, 1.88, and 2.03 for Ω = 60, 90, and 120 rpm, respectively. (b) Expansion of the early time of mixing for Ω = 90 rpm (the same behavior was observed at all rotational speeds). The surfactant used in each case was 15.9 wt % Triton X-405 in water.

[Color figure can be viewed in the online issue, which is available at wileyonlinelibrary.com.]

To examine the kinetics of this fragmentation in our process, we must account for the start of the primary monodisperse emulsion. At the time $t = 0$ s, we do not have an emulsion; the primary monodisperse emulsion is created during the process at a time defined by $t = t_0$ (cf. Figure 3b) and corresponding to a mean drop diameter d_0. This primary monodisperse emulsion is, in fact, the equivalent of the mother emulsion of Mabille et al.[19] Thus, to fit our data, we have to adapt Eq. 8 by introducing t_0 to take into account the time shift and to determine the rupture rate r_0 as follows:

$$d_m(t) = \frac{d_s}{1 - \frac{d_0 - d_s}{d_0}\exp\left(-\frac{r_0(t-t_0)}{3}\right)} \tag{9}$$

t_0, d_0, r_0, and d_s are the free parameters used to fit this model (Eq. 8) with our data using appropriate limit values to fit this equation into the monodisperse regime. Thus, we determine $t_0 = 720$ s, $d_0 = 15.5$ μm, $d_s = 11$ μm, and the rupture rate, $r_0 = 0.0037$ s^{-1}. This value of r_0 is five times smaller than the one found by Mabille et al.[19] for their process. The inverse of r_0 corresponds to the characteristic fragmentation time of 270 s. When compared with the Rayleigh instability, this regime is extremely long; therefore, the two regimes can be decoupled.

This high value of the characteristic fragmentation time is an advantage because it allows the production of different emulsions solely by varying the emulsification time while keeping the same process and the same components. After $t = 2400$ s of mixing, emulsification is achieved and the mean drop diameter remains constant.

Effect of rotational speed on the final diameter

In this section, the surfactant used was also Triton X-405. The composition, the surfactant concentration, the batch TRM geometry, and the protocol used were the same as those previously described. The only variable parameter is the rotational speed of the rod. For each speed studied (Ω = 60, 90, and 120 rpm), the emulsification was performed over 2400 s (40 min) and the power necessary to maintain constant rotational speed was calculated (Eqs. 1 and 2; Figure 6). For the time of 2400 s, the generalized power-law Reynolds numbers (Re_{PL}) associated with each rotational speed are 1.38, 1.88, and 2.03 for Ω = 60, 90, and 120 rpm, respectively, based on the corresponding rheological measurements.

The mean droplet diameter d_m and the uniformity factor U (Eqs. 3 and 5) were determined at different mixing times for each obtained emulsion and for the different rotational speeds (cf. Figure 7). At the beginning of the emulsification, the power rapidly increased until a certain limit, after which time, its value remained nearly constant. This type of behavior has been previously observed by Sanchez et al.[26] for two types of impellers (anchor and helical ribbon) at different rotational speeds. The main difference observed with their results concerns the early stages of mixing, due to the presence in our process of a macromixing step that does not exist in theirs because it represents a pre-emulsification step. This first step can be explained by a lubrication of the rod, leading to a decrease of the measured power. During this macromixing phase, the power remains constant until emulsification begins.

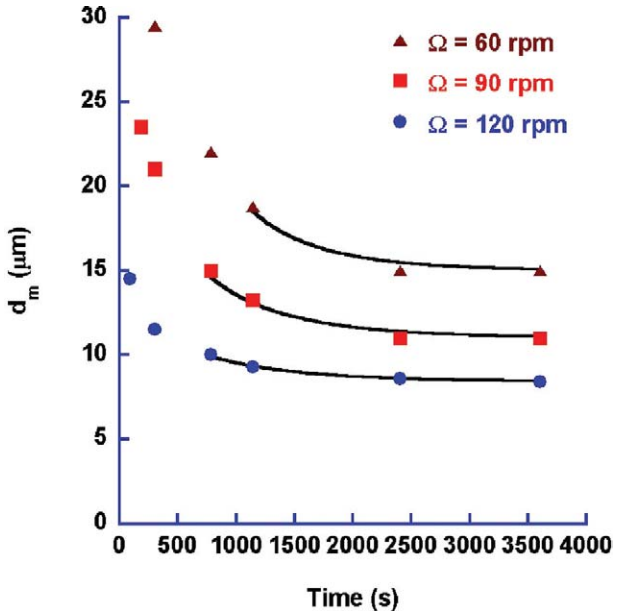

Figure 7. Evolution of the mean droplet diameter during mixing for different rotational speeds.

Ω = 60 rpm (triangles), Ω = 90 rpm (squares), and Ω = 120 rpm (circles). Experimental points were fitted using Eq. 9. [Color figure can be viewed in the online issue, which is available at wileyonlinelibrary.com.]

To fit the experimental data, we adapted the first-order kinetics equation given by Sanchez et al.[26]:

$$P(t) = P_e - P_e \exp[-k(t - t_m)] \tag{10}$$

To take into account the fact that in our process, we have, contrary to Sanchez et al.,[26] a first step in which the power P has an initial value, we adapted Eq. 10 to obtain the following:

$$P(t) = P_e + (P_m - P_e) \exp[-k(t - t_m)] \tag{11}$$

with P_e the final power, k the kinetic constant, t_m the macromixing time, and P_m the power at the end of the macromixing phase. The values of k, P_e, P_m, and P_0 (the initial value of the power before addition of the surfactant mixture) are given in Table 1.

The macromixing time t_m rises exponentially with the reduction in the rotational speed. On the contrary, the kinetic constant k and the final power P_e increase with the rotational speed, as was also observed by Sanchez et al.[26] It is important to note that the power input necessary for the formation of the emulsion was always lower than the initial power P_0 given when only oil is present in the mixer. This can be explained by the fact that for all rotational speeds, the value of shear rate close to the larger rod is around 100 s^{-1} (Figure 5b) and, in this range of shear rates, the viscosity of the final HIPR emulsion is lower than that of the castor oil (as shown hereafter). Thus, the torque applied to the rod to keep the rotational speed constant is lower than that required for the castor oil alone.

For each rotational speed, we determined the mean drop diameter d_m at different mixing times (Figure 7). The experimental data were fitted using Eq. 9 and the different values of r_0, d_s, d_0, and t_0 obtained for each rotational speed are presented in Table 1.

The mean droplet radius decreases with increasing rotational speed of the rod. For all rotational speeds, the evolution of the mean drop diameter can be modeled using Eq. 9, and the rupture rate r_0 remains small regardless of the rotational speed of the rod. The time t_0 when the first monodisperse emulsion is obtained also decreases with increasing rotational speed.

In each case, the mean droplet diameter remains constant after about 2400 s of mixing, and the value of this final droplet diameter is dependent on the rotational speed. A rotational speed of 60 rpm can be used to obtain an emulsion with a mean diameter value ranging between 15 and 30 μm. In contrast, the rotational speed of 120 rpm only permits the production of a mean droplet diameter lower than 15 μm.

Here, we can introduce another characteristic time: $t_{5\%}$, corresponding to the time for which the relative deviation between the mean droplet diameter d_m and the final one d_s is equal to 5% ($d_{5\%} = 1.05\ d_s$). This time is an important one since it could be regarded as the time for which we could consider that emulsification is achieved. Indeed, after this time, the droplet size distribution is almost constant and the very weak variation of the average diameter no longer affects, to any significant degree, the rheological properties of the emulsion. Table 1 gives the characteristic times for each rotational speed studied.

These different characteristic times correspond to the three periods of our emulsification process explained in section "Emulsion preparation." First, during the macromixing time (between $t = 0$ s and $t = t_m$), the introduced water–surfactant mixture lubricates the rod but does not disperse in the oil. Next, from t_m to t_0, the droplets of oil are gradually generated in the water to create the primary monodisperse emulsion. Finally, the fragmentation of the emulsion takes place by reducing the mean droplet diameter until the limit value corresponding to the time $t = t_{5\%}$. The last two periods correspond to the ones observed by Mabille et al.[19]

By integrating Eq. 11 between the macromixing time t_m and a mixing time t, we could determine the evolution of the amount of energy stored in the TRM per unit volume of

Table 1. Values of the Different Parameters Appearing in Eqs. 9 and 11 and of $t_{5\%}$ as Functions of the Rotational Speed

Ω (rpm)	120	90	60
P_0 (W)	6	4	1.7
P_m (W)	1	1.2	0.5
P_e (W)	3.9	2.8	1.4
k (s^{-1})	0.020	0.007	0.004
t_m (s)	6	10	35
r_0 (s^{-1})	0.0035	0.0037	0.0043
d_0 (μm)	10.5	15.5	21
d_s (μm)	8.5	11	15
t_0 (s)	550	720	880
$t_{5\%}$ (s)	1800	2100	2000

dispersed phase, E_{V_d} (energy density in J m^{-3}, Eq. 13) for each rotational speed of the rod:

$$V_d \cdot E_{V_d}(t) = \int_{t_m}^{t} \left\{ P_e - (P_e - P_m) \exp[-k(t - t_m)] \right\} dt \quad (12)$$

$$E_{V_d}(t) = \frac{P_e(t - t_m) + \frac{P_e - P_m}{k} (\exp[-k(t - t_m)] - 1)}{V_d} \quad (13)$$

In this equation, V_d is the volume of the dispersed phase (here, the volume of castor oil). The other parameters have been previously defined. In Figure 8, we plotted the Sauter diameter as a function of the energy density input for the different rotational speeds studied and for emulsification times ranging between t_m and $t_{5\%}$. We have selected these times to account only for the energy used to reach the final mean droplet diameter. During this effective period, the Sauter diameter can be expressed as a function of the energy density using Eq. 14 to fit the experimental data[14]:

$$d_{32} = c \cdot |E_V|^{-b} \quad (14)$$

For each rotational speed, the Sauter diameter decreases with increasing energy density input into the mixer. However, the energy density input necessary to obtain the same value of the Sauter diameter depends on the rotational speed of the rod (cf. Figure 8); likewise, for the same energy density input, the obtained Sauter diameter is dependent upon the rotational speed (cf. Figure 8).

Karbstein and Schubert[13] have obtained HIPR emulsions composed of 80% rapeseed oil (viscosity: 6.1 × 10^{-3} Pa s at 20°C) in water using egg yolk as an emulsifier using different mixers: toothed colloid mill, toothed disc dispersing machine, and high-pressure homogenizer. We found that to obtain emulsions in the TRM having Sauter diameters equivalent to those obtained by Karbstein and Schubert,[13] the necessary energy density seems to be lower in our process. However, the relationship between the Sauter diameter and the energy density also depends upon the composition of the emulsion; thus, this comparison is only indicative. Effectively, to compare the energy efficiency of the TRM to those of other mixers, we must make emulsions with the same components and the same proportions. Furthermore, to calculate the energy density, Karbstein and Schubert[13] used the relation $E_V = \frac{P}{V}$, where V corresponds in this equation to the flow rate of the emulsion.

For high-pressure homogenizers, Stang et al.[14] have obtained energy densities higher than those obtained by our process for different oil/water viscosity ratios (however, their Sauter diameter is smaller ranging between 1 and 15 μm). Once again, this comparison is only indicative because it is made against the literature. The oils and surfactants used in these studies are not the same as the ones used in this study. Also the internal phase concentration is different: the emulsions made with high-pressure homogenizers had an internal phase concentration around 30%.

Effect of surfactant type and concentration

In these experiments, the only variable parameter was the concentration of surfactant used for the emulsification. Two nonionic surfactants are compared: Triton X-100 and Triton X-405. Emulsions were made with a rotational speed of 90 rpm. The emulsification time chosen for the comparison was 780 s (13 min), which corresponds to the end of the first period of evolution of the mean droplet diameter during the mixing (for 15.9 wt % of Triton X-405, see section "Effect of the mixing time on the mean diameter") and to the time at which the power is stabilized. For this time point, the mean droplet diameters were determined and compared (cf. Figure 9).

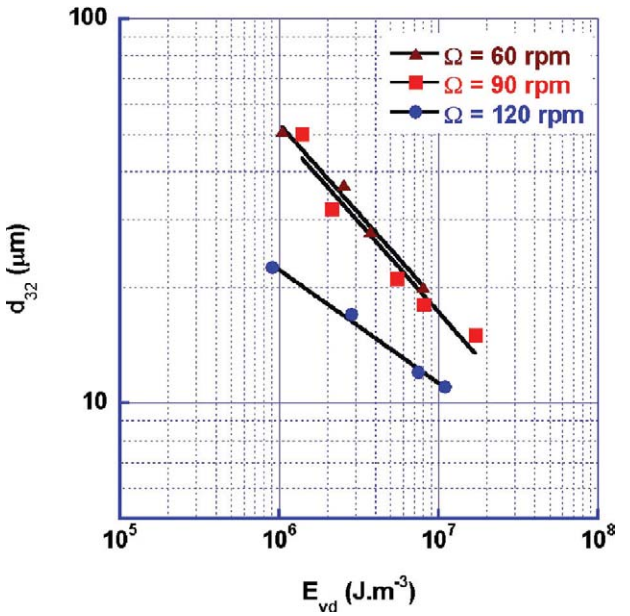

Figure 8. Sauter diameter as a function of energy density E_{V_d} for the different rotational speeds: Ω = 60 rpm (triangles), Ω = 90 rpm (squares), and Ω = 120 rpm (circles).

The values of the couple (c, b) used in Eq. 13 are, respectively: (33,730; 0.5), (32,213; 0.5), and (1288; 0.3). [Color figure can be viewed in the online issue, which is available at wileyonlinelibrary.com.]

For the two studied surfactants, the evolution of the mean droplet diameters presented two regions. In the first time period (region 1), the mean droplet diameter decreased rapidly and in a second one (region 2), this diameter decreased slowly toward an asymptote. These two regions have also been observed by Tcholakova et al.[20] for less concentrated emulsions made using turbulent flow with another nonionic surfactant (Brij 58). These two regions are also called surfactant-poor-region (region 1) and surfactant-rich-region (region 2). The boundary between these two regions could be estimated for a concentration in surfactant about 12 wt % in water for the Triton X-405 and 8 wt % in water for Triton X-100.

For each concentration, emulsions made with Triton X-100 have a mean droplet size smaller than the one of emulsions made with Triton X-405. This could be explained by the fact that the values of the interfacial tension are smaller when Triton X-100 is used, that is, varying between 10^{-3} and 2.10^{-3} N m^{-1} rather than between 4.10^{-3} and 8.10^{-3} N m^{-1} for Triton X-405. For a same concentration of

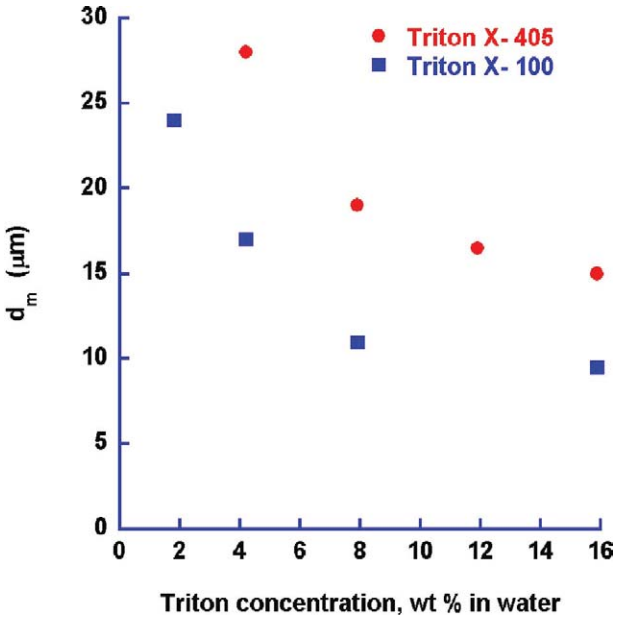

Figure 9. Evolution of the mean droplet diameter as function of the surfactant concentration for emulsions stabilized by Triton X-100 (squares) and Triton X-405 (circles).

[Color figure can be viewed in the online issue, which is available at wileyonlinelibrary.com.]

surfactant, the aqueous solutions have the same viscosity. The addition of Triton surfactant increases the viscosity of the aqueous solution from 10^{-3} Pa s for water to only $6{\cdot}10^{-3}$ Pa s for a concentration of 15.9 wt %. Densities of the various aqueous solutions were found to be close and varying between 1 and 1.02.

The uniformity factor U was also determined for each emulsion via Eq. 5. At low and high concentrations of surfactant, emulsions were unimodal. However, those produced at low concentrations (below 4 wt % of surfactant in water) were unstable. Effectively, coalescence took place after 1 day, whereas emulsions made with higher concentrations of surfactant were quite stable even over a period of several months. According to the definition, emulsion are monodisperse when U is lower or equal to 0.25 and this is the case for all of the HIPR emulsions studied in this section.

Effect of the mean droplet diameter on the rheological behavior

We know that the rheological behavior of emulsions with the same composition is mainly dependent on the droplet size distribution. Thus, to compare the droplet size distributions between two emulsions, we can compare their rheological behaviors.[27] Figure 10 confirms the influence of the mean droplets radius on the rheological behavior of the HIPR castor O/W emulsion obtained in the TRM.

At all values of the mean droplet diameter, the viscosity behaviors of these HIPR emulsions (cf. Figure 10a) are similar and do not present a Newtonian plateau at low shear rates. These emulsions have a shear-thinning behavior in the entire range of the shear rate study. However, there appears to be a break (change in the slope) in this shear-thinning behavior for a shear rate value between 0.1 and 1 s^{-1}. This viscosity behavior is the result of the rearrangement of the droplets, which evolve from a state of equilibrium to a state of flow.[28] Moreover, Figure 10a also illustrates the dependence of the mean droplet size on the viscosity value, and, as

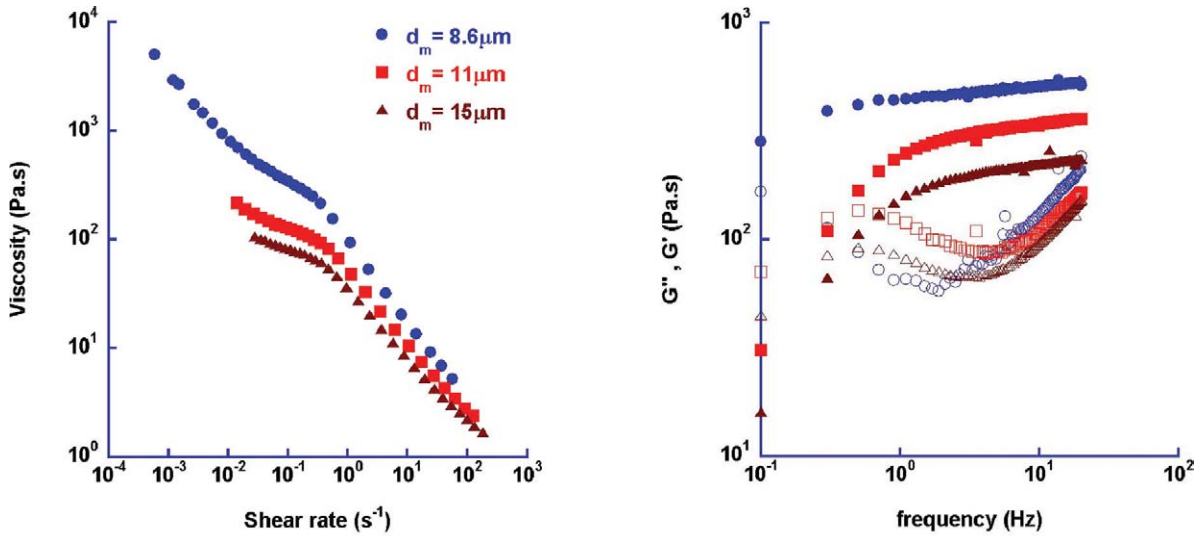

Figure 10. Comparison of the rheological behaviors between HIPR castor oil-in-water emulsions made with Triton X-405 (15.9 wt % in water) for different mean droplet radii: d_m = 8.6 μm (circles), d_m = 11 μm (squares), and d_m = 15 μm (triangles).

(a) Viscosity as a function of shear rate. (b) Evolution of the storage modulus G' (closed symbols) and the loss modulus G'' (open symbols) as functions of frequency for a stress equal to 5 Pa. [Color figure can be viewed in the online issue, which is available at wileyonlinelibrary.com.]

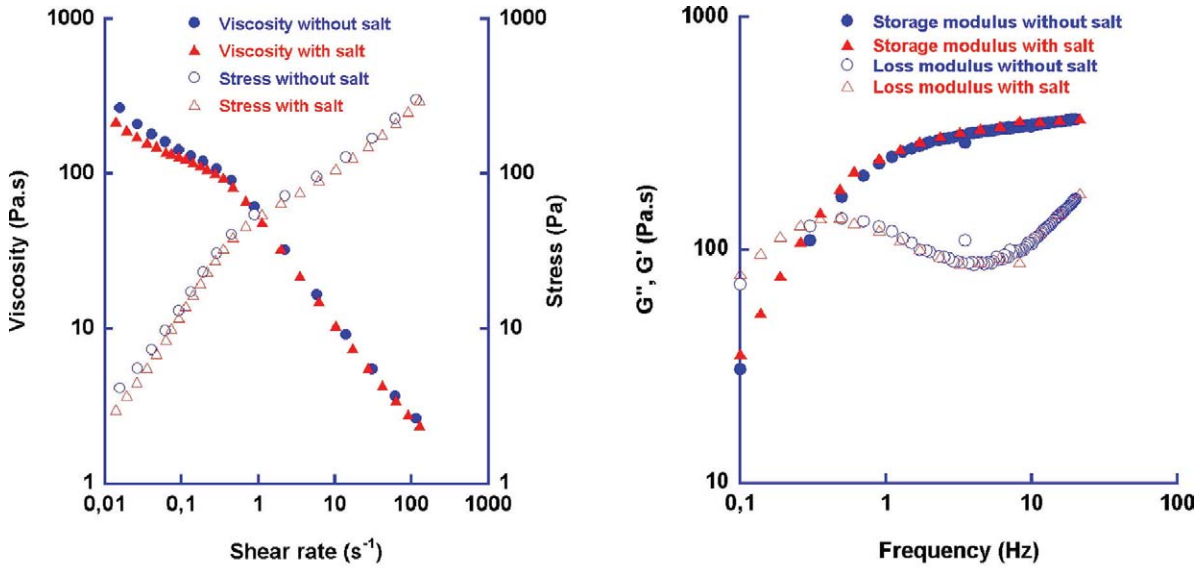

Figure 11. (a) Viscosity (closed symbols) and stress (open symbols) as functions of shear rate for emulsions made with (triangles) and without (circles) salt. (b) Evolution of the storage modulus G' (closed symbols) and the loss modulus G'' (open symbols) as functions of frequency for emulsions made with (triangles) and without (circles) salt.

[Color figure can be viewed in the online issue, which is available at wileyonlinelibrary.com.]

was already observed,[7] the viscosity of the HIPR emulsion increases with decreasing mean droplet radius.

The evolution of the storage modulus G' and of the loss modulus G'' as functions of the frequency observed in Figure 10b was also observed by Mason[29] for HIPR emulsions. At an early time point, the storage modulus increases until it exhibits a plateau, whereas the loss modulus presents a minimum in the frequency band where the storage modulus plateau appears. This minimum is also a manifestation of the rearrangement of the droplets in the HIPR emulsion. In accordance with the results observed by Langenfeld et al.,[27] we note a decrease in the elasticity with increasing mean droplet diameter of the HIPR emulsion.

Effect of salt

Within the context of a targeted application, such as petroleum, biomaterial engineering, pharmaceuticals, cosmetics, etc., it was interesting to evaluate the effect of added salt on the emulsification performance of HIPR emulsion via rheological behavior. An HIPR emulsion made with 30 g/L of salt (corresponding to the average salinity of sea water) in the initial surfactant mixture was compared with one produced classically, both with a rotational speed equal to 90 rpm and with Triton X-405 at a concentration of 15.9 wt % in water.

In section "Effect of the mean diameter on the rheological behavior," we discussed the influence of the mean droplet diameter on HIPR rheological behavior.

Here, we compare the effect of shear rate on the viscosity and the evolution of storage and the loss modulus as functions of frequency between the two HIPR emulsions made with and without salt (cf. Figure 11). As was explained previously, these comparisons permit to indirectly compare the mean droplet diameter of these HIPR emulsions.

Conclusions

We have studied and characterized several parameters affecting the droplet size distributions of HIPR emulsions produced using an original two-rod mixer batch process operating in the highly laminar flow regime (i.e., for a generalized power-law Reynolds number below 2). By adjusting some parameters (stirring time, rotational speed, surfactant type and concentration, and salt addition), we can control the droplet size distribution and thus the rheological and stability characteristics of the created emulsion.

The method used to create the HIPR castor O/W emulsion is a direct one: the oil is in the tank and when the rod is activated to allow the mixture, the solution of water and surfactant is directly introduced and then the HIPR castor O/W emulsion (containing around 90% of internal phase) is made in situ without any intervention contrary to classical batch method used to produce HIPR emulsions for which the internal phase is added slowly. The particularity of this process is the high viscosity ratio of the dispersed phase (castor oil) over the continuous phase (water): $\eta_d/\eta_c = 3400$, whereas the densities are very closed: $\rho_d/\rho_c = 0.974$.

During the emulsification in this TRM batch mixer, the droplet size decreases slowly during the mixing time; thus, it is possible to easily obtain emulsions with targeted mean droplet size (from 30 μm to 6 μm). Here, an initial comparison of droplet size as a function of the energy density input has been made with values found in the literature, although it should be noted that these comparisons should be treated

with caution given that there are variations in the viscosities and the density ratios of the internal and external phases.

Furthermore, the different periods of HIPR emulsification in the TRM have been highlighted, as well as their characteristics times. First, we have a macromixing regime from $t = 0$ s (when the water and surfactant mixture is introduced into the tank) to $t = t_m$. Next, the emulsification begins, and we obtain a first monodisperse emulsion at the time $t = t_0$. Finally, in the last regime, droplets of this initial monodisperse emulsion are gradually broken, and the mean droplet diameter decreases progressively to reach a limit value. Another advantage of the TRM is that the relatively slow rotational speed of the rod (included between 60 and 120 rpm) prevents unsuitable heating of the fluids during the emulsification process. This eliminates the need for a final step of cooling of the emulsion encountered in more classical processes that use turbulent flows with high rotational velocities.

Acknowledgments

The authors gratefully acknowledge Marc Rivaletto and Daniel Champier from the UPPA technical center "Innov'Adour" for their help during the building and the instrumentation of the two-rod mixer batch process. They are also grateful to Dr. R. C. Hiorns for his help to enhance the English language. This work was supported by a Graduate Fellowship (S.C.) from the Communauté d'Agglomération Pau-Pyrénées (CDAPP).

Notation

a = distance between the sensor and the axis, m
C = torque, N m
d_m = mean diameter, μm
d_s = mean diameter of the final emulsion (suturing diameter), μm
d_{32} = Sauter diameter, μm
d_0 = mean diameter of the first monodispersed emulsion, μm
$d_{5\%}$ = 1.05 d_s, μm
d' = tank diameter, mm
d'' = small rod diameter, mm
$\overline{\overline{D}}$ = rate of deformation tensor
E_V = energy density, J m^{-3}
F = strength, N
G' = storage modulus, Pa s
G'' = loss modulus, Pa s
k = consistency index, Pa s^n
P = power, W
P_e = final power, W
P_m = power at the end of the macromixing, W
P_0 = initial value of the power, W
r = larger rod diameter, mm
r_0 = rupture rate, s^{-1}
t = time, s
t_m = macromixing time, s
t_0 = time for which $d_m = d_0$, s
$t_{5\%}$ = time for which $d_m = d_{5\%}$, s
V = volume, m^3
V_f = characteristic flow velocity, $V_f = r \cdot \omega$, m s^{-1}
$\vec{V}$ = velocity vector, m s^{-1}

Greek letters

α = kinetic constant, s^{-1}
ε = larger rod–tank gap, mm
ε' = rod–rod gap, mm
η = dynamic viscosity, Pa s
θ = angular position of the smaller rod, °
ρ = density
μ = mean of the normal distribution
μ_{LN} = mean of the natural logarithms of the log normal distribution
σ = standard deviation of the normal distribution
σ_{LN} = standard deviation of the natural logarithms of the log normal distribution
Ω = rotational speed of the larger rod, rpm
ω = angular velocity of the larger rod, rad s^{-1}

Dimensionless numbers

n = flow behavior index
Re_{PL} = generalized power-law Reynolds number
U = uniformity factor

Subscripts

d = dispersed phase
c = continuous phase

Literature Cited

1. Kizling J, Kronberg B, Eriksonn JC. On the formation and stability of high internal phase O/W emulsions. *Adv Colloid Interface Sci*. 2006;14:295–302.
2. Fournanty S, Le Guer Y, El Omari K, Dejean JP. Laminar flow emulsification process to control the viscosity reduction of heavy crude oils. *J Dispersion Sci Technol*. 2008;29:1355–1366.
3. Princen HM, Aronson MP, Moser JC. Highly concentrated emulsions. II. Real systems. The effect of film thickness and contact angle on the volume fraction in creamed emulsions. *J Colloid Interface Sci*. 1980;75:246–270.
4. Princen HM. Rheology of foams and highly concentrated emulsions. II. Experimental study of the yield stress and wall effects for concentrated oil-in-water emulsions. *J Colloid Interface Sci*. 1985;105: 150–171.
5. Princen HM, Kiss. Rheology of foams and highly concentrated emulsions. IV. An experimental study of the shear viscosity and yield stress of concentrated emulsions. *J Colloid Interface Sci*. 1989;128:176–187.
6. Welch CF, Rose GD, Malotky D, Eckersley ST. Rheology of high internal phase emulsions. *Langmuir*. 2006;22:1544–1550.
7. Malkin AY, Masalova I, Slatter P, Wilson K. Effect on droplet size on the rheological properties of highly-concentrated w/o emulsions. *Rheol Acta*. 2004;43:584–591.
8. Masalova I, Malkin AY, Ferg E, Kharatiyan E, Taylor M, Haldenwang R. Evolution of rheological properties of highly concentrated emulsions with aging-emulsion-to-suspension transition. *J Rheol*. 2006;54:1–17.
9. Cuéllar I, Bullon J, Forgarini AM, Cardenas A, Briceno MI. More efficient preparation of parental emulsions or how to improve a pharmaceutical recipe by formulation engineering. *Chem Eng Sci*. 2005;60:2127–2134.
10. Otsubo Y, Prud'homme RK. Effect of drop size distribution on the flow behaviour of oil-in-water emulsions. *Rheol Acta*. 1994;33:303–306.
11. Yaghi B. Rheology of oil-in-water emulsions containing fine particles. *J Pet Sci Eng*. 2003;40:103–110.
12. Gringras JP, Fradette L, Tanguy P, Jorda E. Concentrated bitumen-in-water emulsification in coaxial mixers. *Ind Eng Chem Res*. 2007;46:1818–1825.
13. Karbstein H, Schubert H. Development in the continuous mechanical production of oil-in-water macro-emulsion. *Chem Eng Process*. 1995;34:205–211.
14. Stang M, Schuchmann H, Schubert H. Emulsification in high-pressure homogenizers. *Eng Life Sci*. 2001;1:151–157.
15. Gringras JP, Fradette L, Tanguy P, Bousquet J. Inline bitumen emulsification using statics mixers. *Ind Eng Chem Res*. 2007;46:2618–2627.
16. Salager JL, Forgiarini A, Marquez L, Pena A, Pizzino A, Rodriguez MP, Rondon-Gonzalez M. Using emulsion inversion in industrial processes. *Adv Colloid Interface Sci*. 2004;108:259–272.
17. Paillet S, Grassl B, Desbrières J. Rapid and quantitative determination of critical micelle concentration by automatic continuous mixing and static light scattering. *Anal Chim Acta*. 2009;636:236–241.
18. Hait SK, Moulik SP. Determination of Critical Micelle Concentration (CMC) of nonionic surfactants by donor-acceptor interaction with iodine and correlation of CMC with hydrophile-lipophile

balance and other parameters of the surfactants. *J Surfactants Deterg*. 2001;4:303–309.
19. Mabille C, Leal-Calderon F, Bibette J, Schmitt V. Monodisperse fragmentation in emulsions: mechanisms and kinetics. *Europhys Lett*. 2003;5:708–714.
20. Tcholakova S, Denkov ND, Danner T. Role of surfactant type and concentration for the mean drop size during emulsification in turbulent flow. *Langmuir*. 2004;20:7444–7458.
21. El Omari K, Le Guer Y. Alternate rotating walls for thermal chaotic mixing. *Int J Heat Mass Transfer*. 2010;53:123–134.
22. El Omari K, Le Guer Y. Thermal chaotic mixing of power-law fluids in a mixer with alternately-rotating walls. *J Non Newtonian*. In press. doi:10.1016/j.jnnFm.2010.03.004
23. Mason TG, Bibette J. Emulsification in viscoelastic media. *Phys Rev Lett*. 1996;77:3481–3484.
24. Hagedorn JG, Martys NS, Douglas JF. Breakup of a fluid thread in confined geometry: droplet-plug transition, perturbation sensivity, and kinetic stabilization with confinement. *Phys Rev E*. 2004;69: 056312.
25. Van Puyvelde P, Vanaroye A, Cardinaels R, Moldenaers P. Review on morphology development of immiscible blends in confined shear flow. *Polymer*. 2008;49:5363–5372.
26. Sanchez MC, Berjano M, Guerrero A, Gallegos C. Emulsification rheokinetics of nonionic surfactant-stabilized oil-in-water emulsions. *Langmuir*. 2001;17:5410–5416.
27. Langenfeld A, Schmitt V, Stébé MJ. Rheological behavior of fluorinated highly concentrated reverse emulsions with temperature. *J Colloid Interface Sci*. 1999;218:522–528.
28. Saiki Y, Prestidge CA. Droplet deformability and emulsion rheology: steady and dynamic behavior. *Korea-Australia Rheol J*. 2005;17: 191–198.
29. Mason TG. New fundamental concepts in emulsion rheology. *Curr Opin Colloid Interface Sci*. 1999;4:231–238.

Manuscript received Sep. 24, 2009, and revision received Feb. 26, 2010.